



Structural and biophysical properties of a [4Fe—4S] ferredoxin-like protein from *Synechocystis* sp. PCC 6803 with a unique two domain structure

Effie Kisgeropoulos^{a,1}, Vivek S. Bharadwaj^{b,1}, Anastasia Ledinina^c, Carolyn E. Lubner^a, David W. Mulder^a, Sharon L. Smolinski^a, Marko Boehm^{d,e}, Kirstin Gutekunst^{d,e}, Paul W. King^{a,*}, Drazenka Svedruzic^{a,*}

^a Biosciences Center, National Renewable Energy Laboratory, Golden, CO 80401, USA

^b Renewable Resources and Enabling Sciences Center, National Renewable Energy Laboratory, Golden, CO 80401, USA

^c Department of Molecular and Structural Biochemistry, North Carolina State University, USA

^d Department of Biology, Botanical Institute, Christian-Albrechts-University, Kiel, Germany

^e Department of Molecular Plant Physiology, Bioenergetics in Photoautotrophs, University of Kassel, Kassel, Germany

ARTICLE INFO

Keywords:

Synechocystis sp. PCC 6803
 Ferredoxin
 Protein structure
 Iron-sulfur clusters
 Redox potentials

ABSTRACT

Electron carrier proteins (ECPs), binding iron-sulfur clusters, are vital components within the intricate network of metabolic and photosynthetic reactions. They play a crucial role in the distribution of reducing equivalents. In *Synechocystis* sp. PCC 6803, the ECP network includes at least nine ferredoxins. Previous research, including global expression analyses and protein binding studies, has offered initial insights into the functional roles of individual ferredoxins within this network. This study primarily focuses on Ferredoxin 9 (slr2059). Through sequence analysis and computational modeling, Ferredoxin 9 emerges as a unique ECP with a distinctive two-domain architecture. It consists of a C-terminal iron-sulfur binding domain and an N-terminal domain with homology to Nil-domain proteins, connected by a structurally rigid 4-amino acid linker. Notably, in contrast to canonical [2Fe—2S] ferredoxins exemplified by PetF (ssl0020), which feature highly acidic surfaces facilitating electron transfer with photosystem I reaction centers, models of Ferredoxin 9 reveal a more neutral to basic protein surface. Using a combination of electron paramagnetic resonance spectroscopy and square-wave voltammetry on heterologously produced Ferredoxin 9, this study demonstrates that the protein coordinates $2 \times [4\text{Fe—4S}]^{2+/1+}$ redox-active and magnetically interacting clusters, with measured redox potentials of -420 ± 9 mV and -516 ± 10 mV vs SHE. A more in-depth analysis of Fdx9's unique structure and protein sequence suggests that this type of Nil-2[4Fe—4S] multi-domain ferredoxin is well conserved in cyanobacteria, bearing structural similarities to proteins involved in homocysteine synthesis in methanogens.

1. Introduction

In photosynthetic organisms, the process of electron transfer is fundamental for converting solar energy into electrochemical and chemical energy. This process requires coordinating multi-component reactions across extensive spatiotemporal networks, resulting in a robust and complex solar conversion system that powers energy conversion reactions. Iron-sulfur (FeS) proteins have an essential role in numerous biological processes and can function as catalysts or electron carriers to support cellular metabolism including photosynthesis, respiration, nitrogen fixation, and stress responses, along with other

functions [1–3]. Ferredoxins, small molecular weight FeS proteins found ubiquitously across species, play a crucial role as electron carriers in energy conversion networks.

The cyanobacterium *Synechocystis* sp. PCC 6803 (S. 6803) serves as a valuable model organism for studying the biochemical components and networks that couple photosynthetic water-oxidation chemistry to reduction-oxidation reactions. The S. 6803 genome encodes nine proteins with characteristic FeS-binding motifs, of which Fdx1 (i.e., PetF, ssl0020) is the most abundant [4–6]. The expression levels of the other eight Fdxs vary depending on environmental conditions, such as fluctuating light, CO₂ concentration, or redox and oxidative stress [4,7].

* Corresponding authors.

E-mail address: drazenka.svedruzic@nrel.gov (D. Svedruzic).

¹ These authors contributed equally.

Some of the better characterized Fdxs include Fdx1, Fdx2 (sl1382), Fdx4 (slr0150) [8], [9–13] and Fdx7 (sl10662) [14,15]. However, there are still substantial gaps in our understanding of their structural and functional characteristics, as well as their roles in biological processes and interactions with protein partners. Most of the Fdxs in *S. 6803* are binding a single [2Fe–2S] cluster, with the exceptions being Fdx7, Fdx8 (ssr3184), and Fdx9 (slr2059), which are predicted to bind [4Fe–4S], [7Fe–8S] and [8Fe–8S] clusters, respectively [4]. Ferredoxins binding [4Fe–4S] clusters are prevalent among anaerobic organisms and generally are more reducing and exhibit greater susceptibility to oxygen, in contrast to the [2Fe–2S] cluster-binding Fdxs.

The objective of this work was to investigate the putative Fdx in *S. 6803*, Fdx9 and determine its essential biophysical properties and function. Fdx9 is expressed at low-abundance and is non-essential under standard photoautotrophic conditions [4]. Based on genetic studies, it is proposed that Fdx9, in conjunction with Fdx7, forms part of the ferredoxin-glutaredoxin-thioredoxin crosstalk pathway, serving a protective role in response to high-light conditions and the presence of toxic metals [4,15]. Using the bacterial adenylate cyclase two-hybrid (BACTH) system, Fdx9 was found to bind in vitro ferredoxin-thioredoxin reductase (FTR) (FtrC, sl10554), flavodiiron protein 3 (Flv3, sl10550), and 3-ketoacyl-acyl carrier protein reductase (FabG, sl10330) [4]. Proteomic studies have revealed the up-regulation of Fdx9 under high-light and low-temperature conditions, alongside other proteins involved in FeS cluster synthesis, respiratory and photosynthetic electron transport, as well as another Fdx (Fdx3, slr1828) [16]. Recent studies of a *S. 6803* Fdx9 deletion strain show diminished growth under photomixotrophic conditions [17].

In summary, Fdx9 is upregulated under growth conditions that lead to redox imbalance and oxidative stress, suggesting a functional role in metabolic pathways that alleviate these stresses. The biophysical and redox properties of Fdx9 and biochemical evidence in support of the proposed functions remain open questions. To address these questions, we expressed heterologously and purified Fdx9 from *S. 6803* and characterized its FeS cluster properties through a combination of electron paramagnetic resonance spectroscopy (EPR) and electrochemistry. The biophysical characterization was complemented by computational analysis of the Fdx9 structure, which suggested that Fdx9 belongs to a unique and poorly characterized group of FeS-containing proteins with two distinct domains: a ligand-binding Nil-domain and a clostridial-type [18] $2 \times [4\text{Fe}–4\text{S}]$ binding domain. The N-terminal domain is a member of the NIL superfamily, which is a suggested substrate-binding domain located in the C-terminal, intracellular region of the MetN subunit of the methionine ABC transporter [19]. The results of this study, along with analysis of available genomic and bioinformatic data, are summarized to propose Fdx9 involvement in the homocysteine synthetic pathways. These findings offer new insights into the roles of two domain $2 \times [4\text{Fe}–4\text{S}]$ proteins in cyanobacterial metabolism and highlight promising avenues for future research in this area.

2. Results and discussion

2.1. Structure and dynamics of Fdx9 in its $2 \times [4\text{Fe}–4\text{S}]$ cluster-bound state

The Fdx9 polypeptide consists of 134 amino acids with molecular

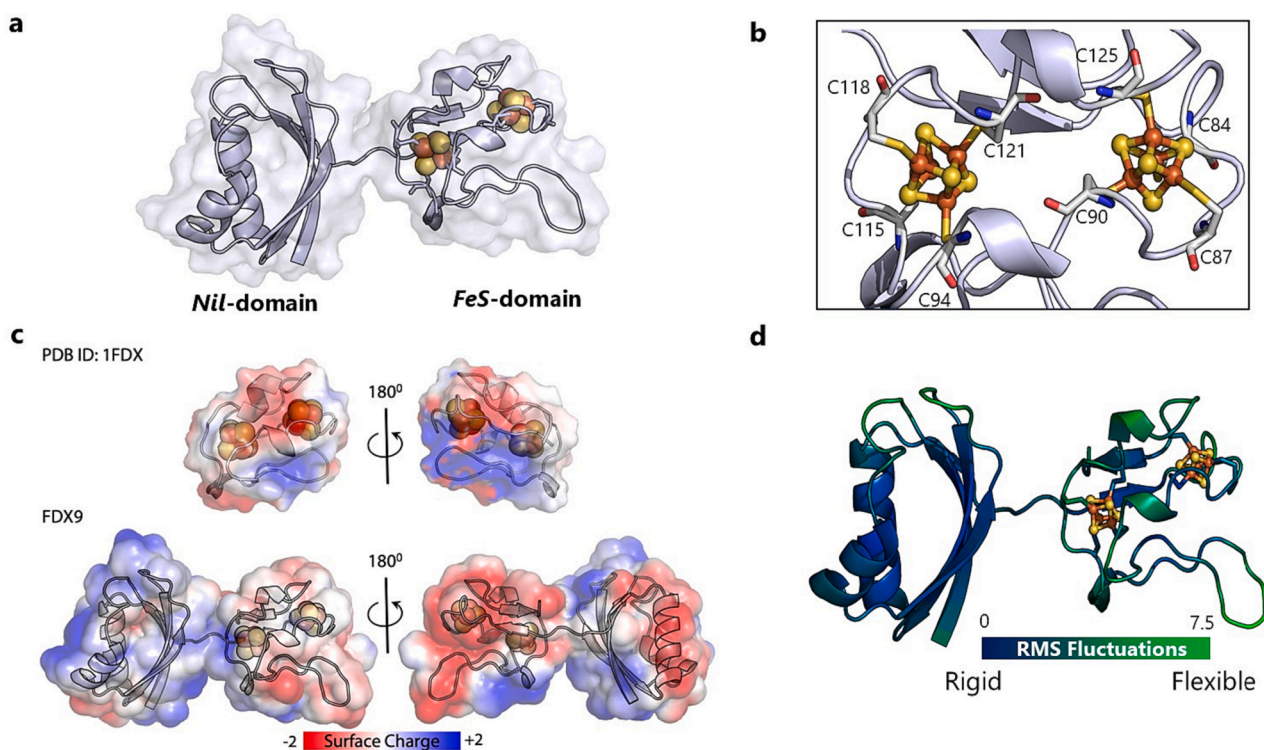


Fig. 1. In silico analysis of Fdx9 structure (a) The putative structure of Fdx9 consists of the Rossmann-like fold Nil-domain [25] and the clostridial-like FeS domain containing $2 \times [4\text{Fe}–4\text{S}]$ clusters. (b) A close-up of the FeS domain depicting the $2 \times [4\text{Fe}–4\text{S}]$ binding domain model showing cysteine residues directly involved in coordinating the clusters. (c) Representation of the electrostatic surface charge distribution Fdx1 (top) and Fdx9 (bottom) calculated using the Adaptive Poisson–Boltzmann Solver (APBS) software. For an easier visual comparison, $2 \times [4\text{Fe}–4\text{S}]$ clusters from Fdx9 are superimposed to Fdx1 structure. For Fdx9, the FeS domain has a more negatively charged surface, while the Nil-domain has a more positively charged surface. (d) Molecular dynamics simulations of the predicted Fdx9 structure under solvated conditions displays structural stability over long simulation time scales (0.5 μs). The blue regions indicate rigid regions with the green regions indicating more flexible regions. The short linker region was observed to be relatively rigid, with the most flexibility shown by a loop on the FeS binding domain. Low flexibility suggests that changes in relative orientations between two domains are unlikely functionally relevant. (For interpretation of the references to colour in this figure legend, the reader is referred to the web version of this article.)

weight of 14.826 kDa⁵. The Fdx9 sequence contains exactly 8 Cys residues, thereby suggesting the presence of two [4Fe-4S] clusters. AlphaFold2 (AF2) was used to predict the structure of Fdx9 based on its amino acid sequence [20]. The predicted AF2 structure revealed two distinct domains connected through a short 4 amino acid linker (Fig. 1a) and was assigned a high confidence score for almost the entirety of the sequence. The N-terminus domain closely resembles a Nil-domain, with a characteristic $\alpha\beta\beta\alpha\beta$ secondary structure. Nil-domains are found at the C-terminus of ABC transporter proteins involved in D-methionine transport as well as in a number of proteins with unknown biological functions [19,21]. The C-terminus domain structure resembles typical $2 \times$ [4Fe-4S] clostridial ferredoxins, with $\beta\alpha\beta\beta\alpha\beta$ fold and typical FeS-binding motif: Cys-X₂-Cys-Gly-X-Cys-X₃-Cys-Pro [3,22]. A comparison to proteins with known crystal structures and two [4Fe-4S] clusters revealed the most significant structural similarities with the C-terminal FeS domain of Fdx9. The single domain ferredoxin structures from *Peptostreptococcus asaccharolyticus* (PDB ID: 1DUR), *Clostridium pasteurianum* (PDB ID: 1CLF), and *Gottschalkia acidurici* (PDB ID: 1FCA), were observed to have the Root Mean Square Deviations (RMSDs) of 0.77, 0.88 and 1.12 Å respectively. The RMSD between corresponding atoms of two protein chains is a commonly used measure of similarity between two protein structures [23]. Any value lower than 2 Å indicates significant structural homology. The RMSDs were calculated based on alignments with the FeS domain of the predicted Fdx9 structure (Fig. S1). Since AF2 does not predict the structures of bound ligands, we modelled the orientation and structure of the two FeS clusters based on these x-ray structures. Specifically, geometry from PDB ID 1FCA was used to generate the cluster bound Fdx9 structure. A close-up of the FeS domain with the cysteine residues involved in coordinating the FeS clusters is shown in (Fig. 1b). Based on the positions of [4Fe-4S] clusters, it is likely that the first [4Fe-4S] cluster (C₈₄...C₈₇...C₉₀...C₁₂₅) is more accessible to potential protein partner(s), while the second is buried, with limited surface accessibility due to position of Nil-domain. This structure was the basis for our molecular dynamics simulations under fully solvated conditions to evaluate its stability, and compare relative flexibilities of loops, alpha-helices and beta sheets within each domain. The structures from these simulations also enable the calculation of surface charge distributions and solvent accessibility (Fig. 1c).

Our simulations indicate a highly stable overall structure that retains secondary structure elements of each individual domain (Fig. 1d). The core structures within each domain were observed to be rigid while the loops on the FeS domain were the most flexible. Surprisingly, the 4-amino acid linker connecting the FeS domain, and the Nil-domain was observed to be structurally rigid (Fig. 1d), which suggests that the relative orientation of Nil- and FeS- domain does not change with changes in functional parameters (e.g., redox state of the cluster or a ligand binding). The two-domain, rigid structure of Fdx9 poses questions about whether it functions in coupling electron transfer to multiple redox carriers and enzymes (e.g., thioredoxin, glutaredoxin, FTR, Flv3) as previously proposed, or has a specific function as an integral part of a multi-subunit enzyme complex.

Ferredoxin-mediated electron transfer complexes are most frequently controlled by electrostatics, where complementarity surface charge has a key role in facilitating binding interactions. Hence, the surface properties of Fdx9 can be informative in predicting binding partners, and in the case of Fdx9, how such binding might affect the relative orientation of the FeS domain with the binding partner to enable electron transfer. The calculated distribution of surface charges for Fdx9 reveals one face of the FeS domain is negatively charged, while another face has a more neutral surface. Such charge distribution of FeS domain differs from that of Fdx1 (Fig. 1c), which has a more predominantly positively charged surface [24], suggesting different protein partners and physiological roles for Fdx1 and Fdx9.

2.2. Fdx9 protein preparation and characterization

UV-Vis absorption spectrum of the reconstituted Fdx9 in the absence of sodium dithionite (DT) showed a broad shoulder centered around ~415 nm, characteristic of [4Fe-4S]²⁺ clusters (Fig. 2a) [18]. Upon Fdx9 exposure to air, noticeable changes in the UV-Vis spectra occurred, with a gradual decrease in the shoulder peak (Fig. 2b), consistent with the high sensitivity of [4Fe-4S] clusters to oxidative conditions. Changes in the spectra did not suggest and orderly transitions to [3Fe-2S] or [2Fe-2S] clusters upon O₂ exposure, and therefore products of cluster degradation were not further investigated. The absorption spectra did not indicate the presence of other optically active cofactors or potentially incorporated ligands within the Nil-domain, although it is noted that the absence of any cofactors could be attributed to the heterologous expression in *E. coli*.

2.3. Characterization of Fdx9 [4Fe-4S] clusters using electron paramagnetic resonance spectroscopy

To analyze the FeS clusters of Fdx9 and identify the predicted presence of $2 \times$ [4Fe-4S] clusters, we performed continuous wave (CW) EPR spectroscopy on reduced Fdx9 (Fig. 3). EPR is commonly used for identifying [4Fe-4S] clusters, which display certain spectral signatures and electron-spin relaxation behavior that can distinguish them from [2Fe-2S] or [3Fe-4S] clusters [26-29]. Prior to the addition of reductant, reconstituted Fdx9 displayed no EPR signals in the $g = 2$ region (Fig. 3a, top). Subsequent reduction of reconstituted Fdx9 with DT indicated the presence of reduced $S = \frac{1}{2}$ [4Fe-4S]⁺ clusters, resulting in the appearance of a complex EPR signal with overlapping features at $g = 1.94, 1.99, 2.01, 2.05$, a shoulder at $g = 2.07$, and broadening at either end (Fig. 3a, bottom). The low-field regions of these samples were also examined for features, such as those originating from higher (i.e., $S > 1/2$) spin-states (Fig. S3a). No such signals were observed in the reduced data, however in the sample of reconstituted Fdx9 prior to reduction we note the presence of an isotropic signal at $g = 4.3$ (Fig. S3a, inset) which is characteristic of high-spin, rhombic Fe³⁺ [30] and is ascribed to a small amount of excess Fe present after FeS cluster reconstitution (see Methods).

To ascertain the relaxation behavior of the reduced Fdx9 spectra, variable-temperature CW EPR experiments were conducted at both 1 mW (Fig. 3b) and 0.1 mW microwave power (Fig. S3b). Similar relaxation behavior was observed at both powers, with temperature saturation evident in the 5 K spectra and maximal signal intensity between 10 and 20 K. Furthermore, the 30 K data display weakened signal intensity and loss of resolution in features across the spectral window (Figs. 3b and S3b). Although there is overlap in the window of temperatures and powers where [4Fe-4S] and [2Fe-2S] clusters are observed, [2Fe-2S] clusters typically exhibit slower relaxation behavior and can be observed free from temperature broadening effects at higher temperatures, while [4Fe-4S] clusters relax more quickly and usually necessitate colder temperatures to observe. In the variable-temperature data collected on Fdx9 we do not observe any shifts in apparent g -values, resolving of signals between 20 K and 30 K, or appearance of new features at 30 K which could be attributed to the presence of an underlying [2Fe-2S] species. Thus, the temperature-dependent behavior of the reduced Fdx9 EPR spectra further supports the presence of [4Fe-4S] clusters and lacks evidence for the presence of [2Fe-2S] clusters. While the relaxation behavior of reduced [3Fe-4S] clusters is less distinct from that of reduced [4Fe-4S] clusters, [3Fe-4S] clusters have an isotropic g -tensor that is quite distinct from the more rhombic g -tensors of [4Fe-4S] clusters. No such signal is observed in the spectra of reconstituted Fdx9 either before or after reduction, consistent with the cluster type assignment of [4Fe-4S].

Nearby [4Fe-4S] clusters, as predicted in Fdx9 by the homology model (Fig. 1), can exhibit a distinct and complex "interaction" type EPR spectrum upon reduction that arises from the presence of magnetic

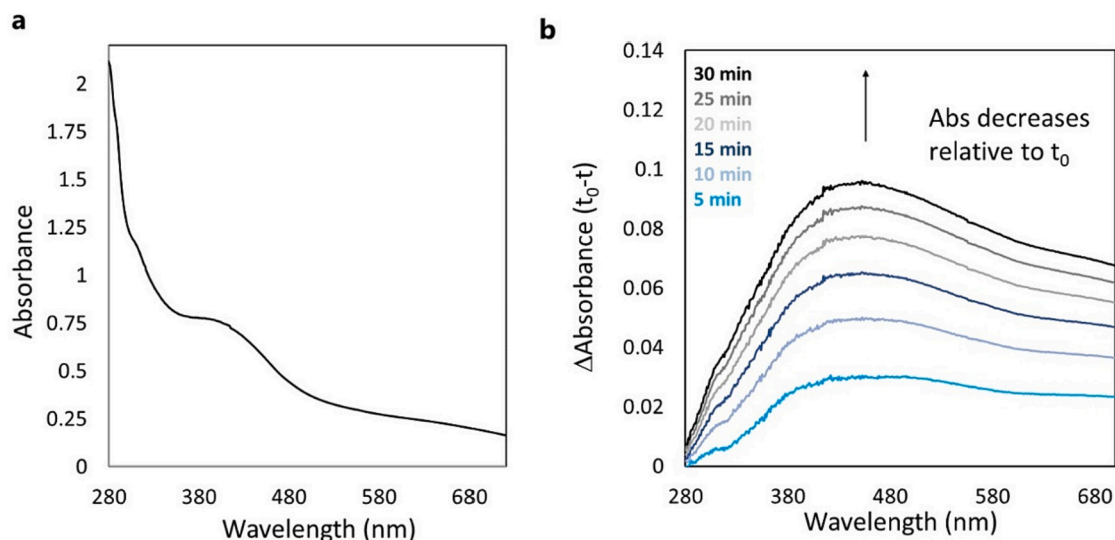


Fig. 2. a) UV-Vis absorption spectrum of reconstituted Fdx9 in the absence of reductant. Ratio of absorbance $A_{280}/A_{415} = 3.4$, after background subtraction (i.e., value at A_{700}). Increased background absorbance can be due to residual FeS particles after protein reconstitution, or precipitated protein. b) Difference absorbance spectra of Fdx9 after exposure to air show the decreased intensity (i.e. increased difference from spectra at $t = 0$ min) of the Fe—S charge transfer bands due to O_2 exposure.

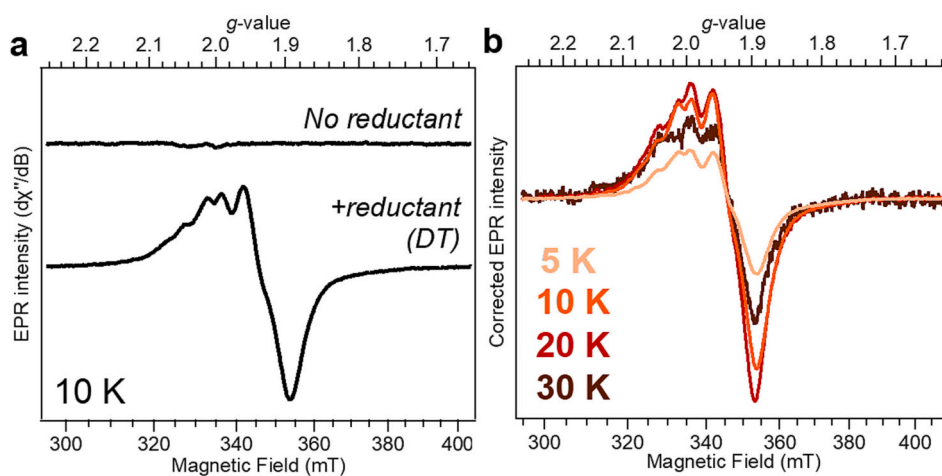


Fig. 3. EPR characterization of reconstituted Fdx9 (a) EPR spectra collected at 10 K of reconstituted Fdx9 either (top) without addition of reductant or (bottom) after subsequent reduction with DT. (b) Variable-temperature EPR spectra of reconstituted, reduced Fdx9 shown after correction for the Curie law (see Methods). EPR data collected using 1 mW of microwave power. EPR spectra were conducted with reconstituted protein (3.9 mg/ml, with $\sim 90\%$ incorporated clusters).

(spin-spin coupling) interactions between two $[4Fe-4S]^+$ clusters [31]. Such interaction signatures have been well documented in similar di-cluster Fdxs and other multi-cluster proteins and include additional features around $g = 2$ and line broadening. Therefore, we hypothesize the complex EPR spectrum of reduced Fdx9 represents the interaction signature arising from two spin-spin coupled $[4Fe-4S]^+$ clusters. This hypothesis was further examined through EPR simulations of reduced Fdx9 which incorporated the addition of an electron-electron spin coupling parameter to reproduce the experimental line-shape (Fig. S3c). Using data collected at 10 K and 1 mW, fitting was first performed using two independent (i.e., non-interacting) $S = \frac{1}{2}$ spin systems (Fig. S3c, Simulation 1). Although the resultant simulation from this model mostly reproduced the Fdx9 signal, two major features around $g = 2$ were unaccounted for. Simulations were then performed using a model of two spin-spin coupled (i.e., interacting) $S = \frac{1}{2}$ spin systems, of either identical or similar g-tensors Fig. S3c, Simulations 2 and 3). These simulations replicated more fully the complexity of the experimental spectrum, in particular those signal features omitted in simulation using a non-

interacting model. Indeed, Simulation 3 shown in Fig. S3c using a magnetic interaction model with slightly different g-tensors for the two clusters, accounts for all major turning points in the reduced Fdx9 spectrum, although the relative positions and (especially) intensities of the features are not fit as well as in Simulation 1. These discrepancies between experimental data and simulation might arise from a need for a rotational matrix to be applied to the coupling matrix, to describe the orientation of the system relative to the molecular frame, or that the g-tensors of the two clusters are distinct at all turning points. Additional simulations and/or collection of multifrequency EPR data will help address this. As a whole, these results are in accordance with the Fdx9 structural model, where the ~ 10 Å distance between $[4Fe-4S]$ clusters, determined through our computational model (Fig. 1b), is within typical distances for the occurrence of spin-spin coupling between paramagnetic centers [32,33]. The presence of spin-spin coupling observed here for Fdx9 signifies a cluster system which is electronically coupled, indicating potential mechanistic implications for tuning of electron transfer rates. Due to the pervasiveness of magnetic (spin-spin coupling)

interactions between clusters in multiple [4Fe–4S] containing proteins such as hydrogenases [34–36], PsaC [37], and other electron transfer proteins [31,38,39], its observance here is thought to be important for the redox properties and functional role of Fdx9.

2.4. Electrochemical properties and redox potentials of the [4Fe–4S] clusters

The redox properties of Fdx9 were further investigated using square wave voltammetry (SWV) with the protein in contact with a pyrolytic graphite edge working electrode (PGE). SWV experiments were conducted by scanning the electrode potential in either reducing (i.e., decreasing potentials) or oxidizing (i.e., increasing potentials) scan directions. During the reduction scans, two overlapping signals were observed with peak potentials of -420 and -520 mV vs. SHE (Fig. 4a). The E_m values fall within the reported range for other $2 \times [4Fe-4S]$ cluster binding proteins, which can vary widely between -280 and -720 mV vs. SHE [3,40]. Repeated scans show some changes in the relative peak intensity and shifts around 10 mV, likely due to protein rearrangement on the electrode surface, which is commonly observed for protein film voltammetry [41]. However, within the applied potential range, repeated scans do not suggest significant irreversible changes or decomposition of $2 \times [4Fe-4S]$ clusters. During the oxidation scans, a clearly visible peak at a potential of -526 mV vs. SHE was observed, along with a low-intensity peak at -420 mV (Fig. 4b). Both values are consistent with the results obtained from the reducing scan experiments. Nevertheless, the relative peak intensities differ significantly, possibly suggesting that the second oxidation step is kinetically limited. The width at half-height of the more intense -526 mV peak is comparable to what is expected for a one-electron redox process (~ 90 mV) [41]. The peak intensities were strongly influenced by the starting potential (Fig. S4). Further investigations and careful consideration of the experimental parameters are essential to gain a comprehensive understanding of the underlying electrochemical processes and to ensure accurate interpretation of the obtained data.

Proteins containing $2 \times [4Fe-4S]$ clusters exhibit intricate electrochemical characteristics owing to the presence of multiple redox-active centers and varying degrees of cluster-cluster interactions. The literature reports various examples of these proteins, including isopotential $2 \times [4Fe-4S]$ proteins [29,40,42], as well as those with significantly different E_m 's [38,40,43], and differing degrees of electronic coupling between clusters [44,45]. The combined results of EPR and SWV suggest that the redox processes in isolated Fdx9 correspond to two electronically coupled [4Fe-4S] clusters. The presence of magnetic coupling (a

representation of electronic coupling) between the two clusters is evident in the EPR spectra of Fdx9, which becomes more complex at potentials closer to -520 mV due to the simultaneous reduction of both clusters. A similar spin delocalized over the two clusters was also observed in the Photosystem I subunit, PsaC [37,46,47] a structurally similar $2 \times [4Fe-4S]$ protein. It is important to acknowledge that E_m values determined in vitro in this work do not necessarily imply that both E_m values are biologically relevant. It is possible that Fdx9 in vivo never exists in a two-electron-reduced state and instead operates as a single-electron acceptor/donor with an E_m value more positive than -520 mV vs. SHE. The interpretation of E_m values and Fdx9 electron transfer mechanism is further complicated by the presence of the Nil-domain, as well as the possibility that Fdx9 is incorporated into redox-active protein complexes, as discussed earlier in the text.

2.5. Discussion about putative protein partners

The investigation into the function of $2 \times [4Fe-4S]$ Fdxs in cyanobacteria represents a compelling research area. This is attributed to their relatively low redox potentials and thermodynamics that are less conducive to photoreduction from PSI particularly when juxtaposed against the more abundant and thermodynamically favorable [2Fe–2S] ferredoxins, which are in addition stable in the presence of O_2 . Based on the two distinct E_m values measured experimentally, we propose two possible models for Fdx9 function: i) Fdx9 is a one electron carrier operating at -420 mV vs. SHE and ii) Fdx9 is 2 electron carrier operating at -420 and -526 mV vs. SHE, as suggested by biophysical characterization (EPR, SWV). In Fig. 4c, we present a visual comparison that illustrates the E_m values of Fdx9, as determined through our study. These E_m values are contrasted with those of other potential redox partners that hold relevance for *S. 6803* metabolism under conditions that are applicable to Fdx9, as established by in vivo studies [4,16,17]. Even though 2 electron reduction of Fdx9 is thermodynamically feasible, utilizing only the higher potential couple in vivo (-420 mV vs. SHE) and engaging in a single electron transfer reactions align better with the redox poise of photoautotrophic metabolism of *S. 6803*, where PSI photoexcitation generates reducing equivalents at E_m values of $-580/-520$ mV vs. SHE. Nevertheless, under more reducing photomixotrophic conditions [17] more reducing E_m should also be considered.

To gain further insights into the potential protein partners, we focused specifically on its unique two-domain Nil- $2 \times [4Fe-4S]$ structure. Using the BLAST sequence alignment tool, we identified sequences of number of unique, wild-type Fdx9 orthologs, primarily from other cyanobacteria ($>80\%$ identity) (Fig. S5). While many of these proteins

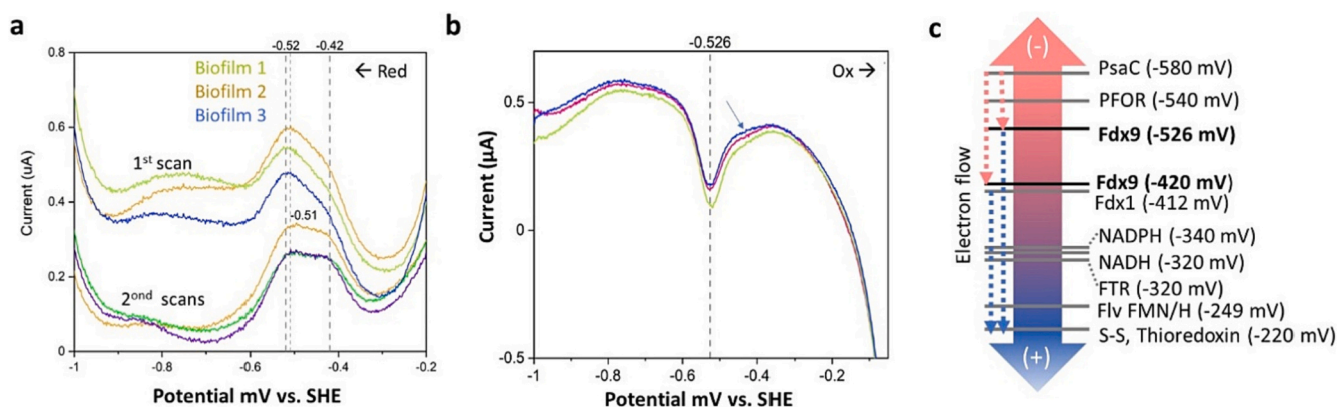


Fig. 4. Square-wave voltammograms of Fdx9 (sample as in Fig. 3). Data was collected with potential applied in both a) reducing and b) oxidizing directions over the -1 to -0.2 or 0 V range, with time in increments of 0.001 V at an amplitude of 0.025 V, a frequency of 10 Hz; under anaerobic conditions, room temperature and pH 8.5. Shifts in E_m values between different experiments likely reflect different protein orientations in biofilms. c) Comparison of redox potentials for Fdx9 measured in this work with biologically relevant protein partners and redox substrates discussed in the text (PsaC [37]; PFOR, pyruvate:ferredoxin oxidoreductase [17]; FTR, ferredoxin:thioredoxin reductase [48]; Flv, flavodiiron; S–S, thioredoxin [3]). Dotted arrows symbolize the direction of electron flow.

remain uncharacterized with unknown biological functions, some were found to be associated with L-aspartate semialdehyde sulfurtransferase (L-ASST) based primarily on genomic and bioinformatic analyses publicly available at *The Universal Protein Resource* (UniProt). L-ASST is an enzyme that catalyzes a redox reaction for the condensation of sulfide with aspartate semialdehyde to produce homocysteine (EC 2.8.1.16). To date, there have been no studies of L-ASST activities in cyanobacteria or connections to ferredoxins. Previous studies on sulfur assimilation in methanogenic archaea have identified two genes, MA1821 and MA1822 from *Methanosarcina acetivorans* (strain ATCC 35395) (*M. acetivorans*), that are essential for homocysteine synthesis [49,50]. Among them, MA1821 encodes an L-ASST (UniProt Q8TPT4), while MA1822 is an associated redox-active protein with Nil-2[4Fe-4S] structure (UniProt Q8TPT3) similar to that of Fdx9. Importantly, their roles in homocysteine synthesis have been experimentally confirmed in two methanogens *M. acetivorans* and *Methanocaldococcus jannaschii* [50,51]. Authors suggested that 2×[4Fe-4S] domain in MA1822 acts as an electron donor during the reduction of disulfide bonds in the conversion of aspartate to homocysteine, whereas the function of the Nil domain remains unclear [51]. Inspired by these findings, we conducted a comparison of sequences and structures for three different Nil-2×[4Fe-4S] proteins: Fdx9 from *S. 6803*, and two putative Fdx9 orthologs: 1) from *Synechocystis* sp. PCC 6714 (D082_02740, UniProt A0A068MUH4) and 2) Fdx9-ortholog from *M. acetivorans* (MA1822, UniProt Q8TPT4) (Figs. S6a,b). Based on the AF2 generated structures, all 3 proteins have the characteristic two-domain structure with Nil and 2×[4Fe-4S] domains (Fig. S6b). Using the String network analysis tool (<http://string-db.org>), potential protein partners with putative L-ASST function for both of the cyanobacterial Fdx proteins were identified (Fig. S6c). A comparison between the identified putative L-ASST from *S. 6803*, *S. 6714* and *M. acetivorans* revealed a high degree of similarity in overall protein sequences and structures (Fig. 5a,b; an extended figure version in Supplemental Fig. S7a,b), as well as the presence of key Cys residues proposed as critical for L-ASST function [50] (Fig. 5a). Moreover, this study benefited from the AF2 generated structures of L-ASST and Fdx9, which facilitated an *in-silico* analysis of the structural feasibility of L-

ASST and Fdx9 complex. The protein-protein complex prediction server Cluspro2 [52,53] was employed for this purpose. Notably, Cluspro provided a plausible structure for the Fdx9-L-ASST complex (Fig. 8a, b), consistent with the hypothesized L-ASST-Fdx9 interaction. However, the full understanding of the functional significance and the precise role of this protein complex requires further investigation through experimental and computational methods.

More broadly, involvement of 2×[4Fe-4S] clusters in disulfide (S-S) chemistry is well-documented for various enzymes, including ferredoxin:thioredoxin reductase (FTR), where a redox-active disulfide is cleaved in sequential one-electron steps to yield two cysteines at the enzyme's active site [48,54]. The E_m values (−526, −420 mV vs SHE), measured for isolated Fdx9 by SWV are consistent with Fdx9 potential involvement in the reduction of disulfide bonds [48], as previously proposed involvement in ferredoxin-glutaredoxin-thioredoxin crosstalk pathway [4]. Further protein-protein network analyses (Figs. S6c and S7c) of the discussed proteins (L-ASSTs and Fdx9 orthologs) suggests their potential involvement in homocysteine and methionine metabolism, specifically strong relationship with methionine synthase (cobalamin-dependent protein MeH in the case of cyanobacteria) and methylenetetrahydrofolate reductase (MTHFR) [55] (Fig. S9). In cyanobacteria, methionine plays critical roles in sensing and protein regulation under redox and oxidative stress conditions [56,57], which is consistent with the conditions leading to Fdx9 expression in response to cellular stress. It is important to emphasize that Fdx9 connection to homocysteine and methionine metabolism is based only on bioinformatic and structure analysis and therefore needs to be experimentally verified.

In a previous study [4] several proteins were identified as potential Fdx9 partners, based on *in vitro* protein-binding assays, including ferredoxin-thioredoxin reductase (FTR) (FtrC, sl10554), flavodiiron protein 3 (Flv3, sl10550), and 3-ketoacyl-acyl carrier protein reductase (FabG, sl10330). Analyses of the available genomic and bioinformatic data have not provided any clues regarding possible interactions between Fdx9 and FTR, Flv3, or FabG, nor ruled them out. Interaction with FTR would be consistent with Fdx9 involvement in redox sensing and

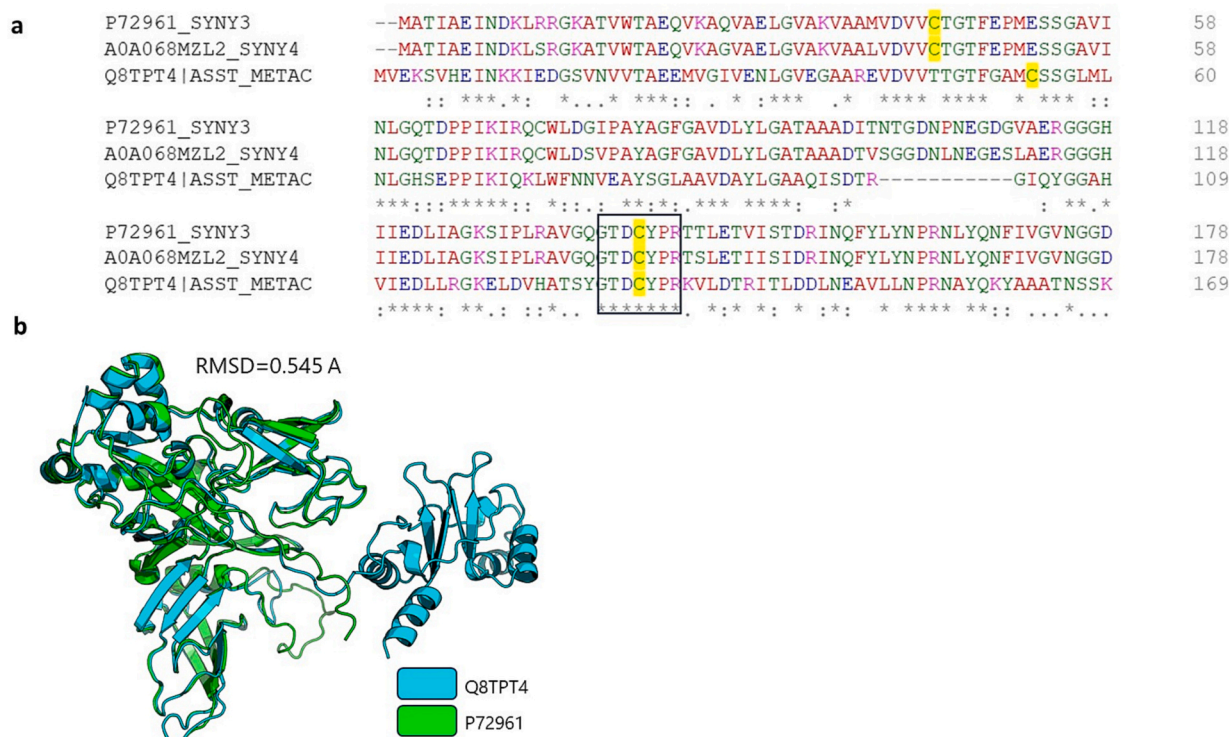


Fig. 5. Comparison of L-ASST orthologs from *S. 6803*, *S. 6714* (and *M. acetivorans* based on data available at:

protein regulation through S—S biochemistry. Interaction of Fdx9 with Flv3 seems inconsistent with Fdx9 O₂-sensitivity reported in this work. Preliminary protein docking studies did not suggest charge transfer interactions between Fdx9 and these proteins (data not shown).

<https://www.uniprot.org/uniprotkb/P72961/entry>; <https://www.uniprot.org/uniprotkb/A0A068MZL2/entry>; <https://www.uniprot.org/uniprotkb/Q8TPT4/entry#structure> a) Comparison of the C-terminal region using Clustal Omega alignment, default settings. Amino acid coloring is as follows: red - small and hydrophobic; blue - acidic; magenta - basic; yellow - cysteine; and green, other polar; box points to putative active site residues (full alignment shown in Fig. S7a); b) AF structures and the alignment of Q8TPT4 (i.e. L-ASST from *M. acetivorans*, MA1822) with P72961 (i.e. putative L-ASST from *S. 6803*) in pymol reveals significant structural similarities as evidenced by an RMSD of ~0.55 Å. MA1822 protein has a distinct domain that is not present in cyanobacterial LASST (also see Fig. S7b).

3. Conclusions

Fdx9 has been classified in the literature as a low-abundant ferredoxin in the *S. 6803* genome. However, characterization here of the atypical Nil- and FeS cluster 2-domain containing protein raises questions about its role as a canonical ferredoxin. Computational analysis and biophysical characterization of heterologously produced Fdx9 confirm the binding of two electronically coupled, redox active [4Fe—4S] clusters. Based on structural characterization, most specifically surface charges, we proposed that Fdx9 is not directly involved in charge transfer with PSI. Based primarily on bioinformatic and in silico analysis, we propose that L-ASST is a protein partner with Fdx9. However, further experimental studies are required to test our hypothesis. In summary, our findings deepen our understanding of the functional roles played by proteins containing 2×[4Fe—4S] clusters in photosynthetic organisms, especially considering their O₂ sensitivity. The optimization of photosynthetic activities, particularly in terms of their redox and oxidative stress responses, holds paramount importance for the effective utilization of photosynthetic organisms in carbon capture, biofuel production, and the synthesis of valuable biochemicals.

4. Materials and methods

4.1. Computational structure analysis

The atomistic structure of Fdx9 was predicted using the open-source neural-network-based protein prediction tool AlphaFold2 [22]. This structure formed the basis for the surface charge analysis and molecular dynamics simulations conducted in this study. The Adaptive Poisson Boltzmann Solver v.1.5 was used to evaluate the distribution of charges on the Fdx9 surface [58]. The protocol involved converting the pdb file to a .pqr format that contains the protonation states and atomic charges for each atom in the system this .pqr file is then inserted into the APBS program to generate surface charges. The surface charge distributions were plotted using pymol. The predicted structure of Fdx9 was also tested for stability using molecular dynamics simulations in a fully solvated environment with both [4Fe-4S] clusters ligated to the cysteine residues. One [4Fe—4S] cluster (residue 135) involved C84, C87, C90 and C125 while the other (residue 136) involved C94, C115, C118 and C121. The amber ff14SB forcefield was employed for the protein and the TIP3P forcefield for the water molecules, Na⁺ and Cl⁻ ions were added to ensure charge neutrality. The parameters for the [4Fe—4S] cluster and the coordinating cysteine residues were obtained from Caravallho et al. [58,59] The cluster was considered with an overall spin of S = 0 and with an oxidation state of +2 i.e. [Fe₄-S₄]⁺². After an initial equilibration for 200 ps, the solvated cluster-bound enzyme was simulated in the NVT ensemble for 500 ns. The predicted structure was observed to be stable over the simulation and root mean square fluctuations were then calculated to explore relative flexibilities of the

structural domains.

4.2. Cloning and expression

The *fdx9* gene from *Synechocystis* sp. PCC 6803 [a slr2059] was codon-optimized and synthesized for expression in *E. coli* by Genscript, USA. A strep-tag with three amino acid linker was placed at the C-terminus of the DNA sequence with amino acid sequence [GSAWSHPQFEK], with corresponding nucleotide sequence [ggcagcgcgtggagccaccgcagtttgagaag]. This gene was subcloned into the pCDF Duet-1 vector utilizing the *EcoRI* and *HindIII* restriction sites. All plasmids constructed were verified by commercial sequencing (Genscript, USA). The heterologous expression of Fdx9 was carried out in *E. coli* BL21(DE3) cells. A 1:100 overnight culture was utilized to inoculate 1 L of terrific broth placed in 2 L flasks, with the following additives: 1 ml 1000× trace metals mix (50 mM FeCl₃, 20 mM CaCl₂, 10 mM MnCl₂, 10 mM ZnSO₄, 5 mM MgSO₄, 2 mM CuCl₂, 2 mM NiCl₂), 0.4% glycerol, 125 μg mL⁻¹ thiamine-HCl, and 100 μg mL⁻¹ Streptomycin. Cells were grown at 37 °C and 250 rpm until an optical density of ~0.6 at 600 nm was reached. The culture was then inoculated with a final concentration of 1.0 mM IPTG and 2.5 mM ferric ammonium citrate. Cultures were grown for another hour in the shaker after which two 1 L cultures were combined into 2 L septum sealed flasks, with addition of 10 mM sodium fumarate and 0.5% w/v D-glucose, and stored stationary at room temperature for 30 min. Afterward, L-cysteine was added to a concentration of 1 mM and cultures were sparged with argon gas overnight at room temperature. Cells were harvested anaerobically via centrifugation and cell pellets were resuspended in 50 mM TRIS pH 8.5 with 50 mM NaCl and 5% glycerol before storage in septum-sealed vials -80 °C. When expressed under aerobic conditions, Fdx9 exhibited low yields and mostly insoluble protein.

4.3. Protein preparation and analysis

Cell lysis and protein purification were carried out anaerobically. Cell cultures were thawed and mixed with 75 units of Pierce Universal Nuclease, 20 mg lysozyme, and 1 tablet of Roche cOmplete EDTA-Free Protease Inhibitor Cocktail. Lysis was accomplished using a Microfluidics M-110S microfluidizer and clarified via ultracentrifugation at 45,000 rpm for one hour at 4 °C. Supernatant was transferred onto a gravity column containing high-capacity Strep-Tactin XT-4Flow resin (IBA Life Sciences) previously equilibrated with 10 CV buffer. The column was washed with a 5 column-volume (CV) buffer and eluted with 5 CV buffer containing 25 mM D-Biotin pH 8.5. Eluant was quantified by Bradford method with a correction factor of 2.05, which was determined by comparing the calculated concentration based on the theoretical Expiry extinction coefficient of 12,990 M⁻¹ cm⁻¹ at 280 nm before reconstitution of clusters with the calculated concentration based on Bradford method. Typical yields were ~ 2 to 3.5 mg protein per L of cell culture. Quantification of iron was performed utilizing previously published methods [60]. Post purification Fdx9 contained about 30% of its prescribed 2×[4Fe—4S] clusters and required in vitro reconstitution. Reconstitution reaction was performed in an anaerobic chamber. A reaction containing 150 μM Fdx9 was slowly combined with 1% β-mercaptoethanol and stirred for 30 min at room temperature. After which 300 μM ferrous ammonium sulfate was slowly added. After 15 min of stirring, 300 μM of sodium sulfide was added in the same manner and stirred for another 15 min. The reaction was incubated at 4 °C for 14–18 h. Removal of excess reagents was completed by desalting the reconstitution reaction with PD-10 desalting columns (GE Life Sciences). Protein was concentrated as appropriate with ultrafiltration via an Amicon Stirred Cell with 1 kD cutoff filter. To ensure complete iron loading, the purified Fdx9 was reconstituted under anaerobic conditions. On average, the iron loading for multiple protein preparations was 77 ± 30%. The % of iron was calculated based on the expected value of 8 Fe per protein. Protein samples with the highest Fe content were used for

the experiments.

4.4. UV/Visible absorption experiments

Measurements were carried out by taking spectra of Fdx9 in 50 mM TRIS pH 8.5, 50 mM NaCl, 5% glycerol under anaerobic conditions in septum-sealed 10 mm quartz cuvettes at room temperature on a Cary 4000 UV–visible spectrophotometer. O₂ sensitivity experiments were conducted by exposing cuvette to air.

4.5. Electron paramagnetic resonance experiments

EPR samples of Fdx9 were prepared in a glovebox under anaerobic conditions (Mbraun, N₂ atmosphere) from reconstituted Fdx9 (in 50 mM Tris, 50 mM NaCl, 5% glycerol, pH 8.5 buffer) either prior to the addition of reductant (no reductant) or after reduction using DT (Figs. 3a and S3a). To generate the reduced sample of reconstituted Fdx9, DT from a 100 mM stock was added to Fdx9 at a final concentration of 5 mM DT. Samples were prepared at 100 μM, with ~200 μL loaded anaerobically into EPR tubes (Wilmad 707-SQ-250) and frozen with liquid N₂. Spectra were collected on samples from two separate, reconstituted preparations of Fdx9 protein, which displayed similar signals and temperature dependent properties in the $g = 2$ region and at low field. Qualitative assessment of the EPR spectra at temperatures above 30 K showed continued temperature broadening and relaxation of the low-temperature signals with no additional signals. The isotropic signal at $g = 4.3$ observed in reconstituted Fdx9 samples prior to reduction (Fig. S3a) is characteristic of high-spin, rhombic Fe³⁺ species, [30] as might be found after FeS cluster reconstitution from excess Fe. However, this signal is only observed in the reconstituted sample prior to reduction, and disappears after introduction of 5 mM DT. This along with the low signal area of the feature (especially relative to the total signal area of the reduced sample) indicates a relatively small population of this Fe³⁺ species. We also note that while FeS cluster reconstitution can likewise result in excess Fe precipitated out as insoluble FeS, this form would not contribute an EPR signal.

4.5.1. Data collection and processing

X-band (9.38 GHz) CW EPR data were collected on an Elexsys E500 spectrometer equipped with a super high-Q resonator (Bruker, USA), cryogen-free helium system (ColdEdge Technologies, USA), and MercuryTC temperature controller (Oxford Instruments, UK). Data were collected at powers and temperatures indicated in figure captions, using a modulation frequency of 100 kHz and modulation amplitude of 10 G. Spectra were background corrected through the subtraction of buffer spectra. When necessary, additional baseline correction was applied by subtraction of a polynomial function in IgorPro v.9. Temperature dependent data were not baseline corrected prior to their respective normalization.

4.5.2. Data analysis and simulation

To obtain the temperature-normalized spectra for relaxation behavior analysis (Figs. 3b and S3b), variable-temperature CW data were corrected for dependence on the Curie law through multiplication of the spectra by the respective collection temperatures. EPR simulations were performed using the EasySpin toolbox [61] and its core function “pepper” within Matlab version R2020A (MathWorks). Spectra were max/min normalized prior to fitting and simulation. Simulation of data was first performed using two components with rhombic g -tensors that were allowed to float during fitting, yielding g -tensors of $g_{FS1} = [2.047 \ 1.948 \ 1.873]$ and $g_{FS2} = [2.081 \ 1.923 \ 1.892]$ with g -strain values of $gStrain_{FS1} = [0.03 \ 0.02 \ 0.02]$ and $gStrain_{FS2} = [0.03 \ 0.035 \ 0.02]$ (Fig. S3c, Simulation 1). Simulations treating the clusters as magnetically interacting were then attempted through inclusion of the electron-electron interaction term in the spin-Hamiltonian (Fig. S3c, Simulations 2 and 3). This was achieved by invoking the EasySpin spin system

parameter Sys.ee, which represents the total coupling matrix and is given (in MHz) as three numbers which correspond to the principal values making up the diagonal of the interaction matrix. Simulation 2 of Fig. S3c shows the data simulated using two components with identical rhombic g -tensors ($g_{FS1} = g_{FS2} = [2.060 \ 1.960 \ 1.885]$) and g -strain ($gStrain_{FS1} = gStrain_{FS2} = [0.025 \ 0.02 \ 0.02]$) and a coupling matrix of $ee = [281 \ 40, 267]$. Although this improved the quality of the fit overall by beginning to replicate the spectral complexity, it did not reproduce all the turning points and additional attempts were made to simulate the data allowing variation in the g_2 value for each tensor along with the coupling matrix. Simulation 3 of Fig. S3c is the result of this, with $g_{FS1} = [2.06 \ 1.98 \ 1.885]$, $g_{FS2} = [2.06 \ 1.94 \ 1.885]$, $gStrain_{FS1} = gStrain_{FS2} = [0.02 \ 0.015 \ 0.015]$, and $ee = [300100267]$.

4.6. Square wave voltammetry

Protein-film square-wave voltammetry (SWV) measurements were performed to assess the reduction potentials of the two [4Fe-4S] clusters of Fdx9. A three-electrode 100 mL standard cell (Pine Research) apparatus comprised of a non-rotating, fixed disk pyrolytic graphite edge (PGE) working electrode (Pine Research), low profile Ag/AgCl/saturated potassium chloride reference electrode (Pine Research), and platinum wire counter electrode (BASi) was utilized for these experiments. The electrode was polished using an alumina slurry (BASi) and alumina polishing pads (BASi) and rinsed thoroughly prior to application of the protein film. Fdx9 was adsorbed to the electrode by application of 5 μL concentrated protein solution and left to incubate for at least 10 min with subsequent washing with buffer (50 mM TRIS pH 8.5, 50 mM NaCl, 5% glycerol). Experiments were carried out in a minimum of three replicates in an anaerobic chamber (MBraun) with buffer in the standard cell while stirring at room temperature. Data was collected with potential (E) applied in both the oxidizing and reducing directions over the -1.2 to 0 V range, with time in increments of 0.001 V at an amplitude of 0.025 V, a frequency of 10 Hz, and using a sensitivity setting of $1 \times 10^{-6} \text{ A} \cdot \text{V}^{-1}$ with a CH Instruments 630C potentiostat and CHI630C software. Buffer background measurements were achieved by scans performed under the same conditions, but with omission of the protein film. All potential values are reported versus SHE is following conversion from the Ag/AgCl/saturated potassium chloride reference electrode by addition of 199 mV.

4.7. Sequence analysis and alignment

We have used a series of publicly available bioinformatic tools to study proteins' structure and function. BLAST was used for sequence similarity searches and inferring protein function (>80% identity, >230 Total score), UniProt (<https://www.uniprot.org/uniprotkb/P73811/entry>) (<https://www.uniprot.org/uniprotkb/P73811/entry>) was used for annotated information for Fdx9 and selected ferredoxins and L-ASST, Clustal Omega was used for multiple protein sequence alignments using default settings, STRING to identify protein-protein interactions and functional associations, and KEGG was used to investigate biological context and pathways potentially involving L-ASST.

Author statement

We, the authors of this manuscript, wish to convey the following key points:

Research contribution and significance

This study presents original research that significantly contributes to the field of Inorganic Biochemistry. It offers novel insights into the role of [4Fe4S]-cluster binding electron carrier proteins in photosynthetic organisms, and more specifically their response to redox and oxidative stress. Protein in this study, was previously classified as a low-abundant

ferredoxin in *Synechocystis* sp. PCC 6803. We found that it exhibits a unique two-domain structure. Comprehensive computational and biophysical characterization brings into question its role as canonical ferredoxin.

Author contributions

Each author has made substantial contributions to this research. A.L., C.E.L., M.B., and D.S. collaborated on protein preparations and characterizations; A.L., C.E.L., and D.S. conducted and interpreted square wave voltammetry measurements, D.W.M and E.K. contributed by collecting EPR data, conducting data analysis, and performing simulations; V.S.B., conducted computational modeling including structure prediction, charge distribution analysis, and molecular dynamics simulations; S.L.S and M.B. contributed to the protein function analysis and biochemical assays; P.W.K. and D.S. conceptualized the project and oversaw the overall effort. All authors contributed to manuscript preparation and editing.

Ethical considerations

This research adhered to all relevant ethical guidelines as determined by Department of Energy, and received necessary approvals from National Renewable Energy Laboratory leadership.

Declaration of Competing Interest

None of the co-authors received any financial or non-financial assistance provided by a third party for the reported work.

None of the co-authors have any financial interest or relationship related to the subject matter directly or indirectly related to this manuscript.

This work is not pending any patents or copyrights.

Data availability

The data and materials supporting this research are available upon request. [Provide contact information or indicate where the data can be accessed, e.g., in a repository]. We appreciate the opportunity to submit our work for consideration in Journal of Inorganic Biochemistry. We believe that our research aligns well with the journal's focus and would be of interest to its readership.

Acknowledgements

This work was authored by the National Renewable Laboratory, operated by Alliance for Sustainable Energy, LLC, for the U.S. Department of Energy (DOE) under Contract No. DE-AC36-08GO28308. Funding provided by the U.S. Department of Energy Office of Basic Energy Sciences, Division of Chemical Sciences, Geosciences, and Biosciences, Photosynthetic Systems Program. The views expressed in the article do not necessarily represent the views of the DOE or the U.S. Government. The U.S. Government retains and the publisher, by accepting the article for publication, acknowledges that the U.S. Government retains a nonexclusive, paid-up, irrevocable, worldwide license to publish or reproduce the published form of this work, or allow others to do so, for U.S. Government purposes.

Appendix A. Supplementary data

Supplementary data to this article can be found online at <https://doi.org/10.1016/j.jinorgbio.2023.112428>.

References

- [1] G.T. Hanke, Y. Satomi, K. Shinmura, T. Takao, T. Hase, A screen for potential ferredoxin electron transfer partners uncovers new, redox dependent interactions, *Biochim. Biophys. Acta (BBA) - Proteins Proteom.* 1814 (2011) 366–374.
- [2] G. Hanke, P. Mulo, Plant type ferredoxins and ferredoxin-dependent metabolism, *Plant Cell Environ.* 36 (2013) 1071–1084.
- [3] J.T. Atkinson, I. Campbell, G.N. Bennett, J.J. Silberg, Cellular assays for ferredoxins: a strategy for understanding Electron flow through protein carriers that Link metabolic pathways, *Biochemistry* 55 (2016) 7047–7064.
- [4] C. Cassier-Chauvat, F. Chauvat, Function and regulation of ferredoxins in the cyanobacterium, *Synechocystis* PCC6803: recent advances, *Life* 4 (2014) 666–680.
- [5] Y. Nakamura, T. Kaneko, M. Hirotsawa, N. Miyajima, S. Tabata, CyanoBase, a www database containing the complete nucleotide sequence of the genome of *Synechocystis* sp. strain PCC6803, *Nucleic Acids Res.* 26 (1998) 63–67.
- [6] T. Kaneko, et al., Sequence analysis of the genome of the unicellular cyanobacterium *Synechocystis* sp. in: *Strain PCC6803. II. Sequence Determination of the Entire Genome and Assignment of Potential Protein-Coding Regions* vol. 3, DNA Research, 1996, pp. 109–136.
- [7] A.K. Singh, et al., Integrative analysis of large scale expression profiles reveals core transcriptional response and coordination between multiple cellular processes in a cyanobacterium, *BMC Syst. Biol.* 4 (2010) 105.
- [8] H. Bottin, B. Lagoutte, Ferredoxin and flavodoxin from the cyanobacterium *Synechocystis* sp PCC 6803, *Biochim. Biophys. Acta (BBA) - Bioenerg.* 1101 (1992) 48–56.
- [9] K. Mazouni, F. Domain, F. Chauvat, C. Cassier-Chauvat, Expression and regulation of the crucial plant-like ferredoxin of cyanobacteria, *Mol. Microbiol.* 49 (2003) 1019–1029.
- [10] K. Gutekunst, et al., The bidirectional NiFe-hydrogenase in *Synechocystis* sp. PCC 6803 is reduced by flavodoxin and ferredoxin and is essential under mixotrophic, nitrate-limiting conditions, *J. Biol. Chem.* 289 (2014) 1930–1937.
- [11] M. Poncet, C. Cassier-Chauvat, X. Leschelle, H. Bottin, F. Chauvat, Targeted deletion and mutational analysis of the essential (2Fe–2S) plant-like ferredoxin in *Synechocystis* PCC6803 by plasmid shuffling, *Mol. Microbiol.* 28 (1998) 813–821.
- [12] T. Motomura, et al., An alternative plant-like cyanobacterial ferredoxin with unprecedented structural and functional properties, *Biochim. Biophys. Acta (BBA) - Bioenerg.* 1860 (2019), 148084.
- [13] M. Schorsch, et al., A unique ferredoxin acts as a player in the low-iron response of photosynthetic organisms, *Proc. Natl. Acad. Sci.* 115 (2018) E12111–E12120.
- [14] H. Mustila, Y. Allahverdiyeva, J. Isojärvi, E.M. Aro, M. Eisenhut, The bacterial-type [4Fe–4S] ferredoxin 7 has a regulatory function under photooxidative stress conditions in the cyanobacterium *Synechocystis* sp. PCC 6803, *Biochim. Biophys. Acta (BBA) - Bioenerg.* 1837 (2014) 1293–1304.
- [15] C. Cassier-Chauvat, F. Chauvat, Responses to oxidative and heavy metal stresses in cyanobacteria: recent advances, *Int. J. Mol. Sci.* 16 (2015) 871–886.
- [16] S.-J. Hong, et al., Proteomic analysis of *Synechocystis* sp. PCC6803 responses to low-temperature and high light conditions, *Biotechnol. Bioprocess Eng.* 19 (2014) 629–640.
- [17] Y. Wang, et al., Pyruvate:ferredoxin oxidoreductase and low abundant ferredoxins support aerobic photomixotrophic growth in cyanobacteria, *Elife* 11 (2022).
- [18] J. Liu, et al., Metalloproteins Containing Cytochrome, Iron–Sulfur, or Copper Redox Centers, *Chem. Rev.* 114 (2014) 4366–4469.
- [19] N.S. Kadaba, J.T. Kaiser, E. Johnson, A. Lee, D.C. Rees, The high-affinity *E. coli* methionine ABC transporter: structure and allosteric regulation, *Science* 321 (2008) 250–253.
- [20] J. Jumper, et al., Highly accurate protein structure prediction with AlphaFold, *Nature* 596 (2021) 583–589.
- [21] <https://www.ebi.ac.uk/interpro/entry/InterPro/IPR018449/>.
- [22] N. Nzuzi, et al., Diversification of ferredoxins across living organisms, *Curr. Issues Mol. Biol.* 43 (2021) 1374–1390.
- [23] B.A. Reva, A.V. Finkelstein, J. Skolnick, What is the probability of a chance prediction of a protein structure with an rmsd of 6 Å? *Fold. Des.* 3 (1998) 141–147.
- [24] J. Li, et al., Structure of cyanobacterial photosystem I complexed with ferredoxin at 1.97 Å resolution, *Communicat. Biol.* 5 (2022) 951.
- [25] K.E. Medvedev, L.N. Kinch, R.D. Schaeffer, N.V. Grishin, Functional analysis of Rossmann-like domains reveals convergent evolution of topology and reaction pathways, *PLoS Comput. Biol.* 15 (2019), e1007569.
- [26] H. Rupp, K.K. Rao, D.O. Hall, R. Cammack, Electron spin relaxation of iron-Sulphur proteins studied by microwave power saturation, *Biochim. Biophys. Acta (BBA) - Protein Struct.* 537 (1978) 255–269.
- [27] R. Cammack, F. MacMillan, in: G. Hanson, L. Berliner (Eds.), *Metals in Biology: Applications of High-Resolution EPR to Metalloenzymes*, Springer, New York, New York, NY, 2010, pp. 11–44.
- [28] W.R. Hagen, EPR spectroscopy of complex biological iron–sulfur systems, *JBC J. Biol. Inorg. Chem.* 23 (2018) 623–634.
- [29] O. Guerrini, et al., Characterization of two [2Fe4S] ferredoxins from *Clostridium acetobutylicum*, *Curr. Microbiol.* 56 (2008) 261–267.
- [30] F. Bou-Abdallah, N.D. Chasteen, Spin concentration measurements of high-spin (g' = 4.3) rhombic iron(III) ions in biological samples: theory and application, *J. Biol. Inorg. Chem.* 13 (2008) 15–24.
- [31] R. Mathews, S. Charlton, R.H. Sands, G. Palmer, On the nature of the spin coupling between the Iron-sulfur clusters in the eight-Iron ferredoxins, *J. Biol. Chem.* 249 (1974) 4326–4328.
- [32] C.C. Page, C.C. Moser, X. Chen, P.L. Dutton, Natural engineering principles of electron tunnelling in biological oxidation–reduction, *Nature* 402 (1999) 47–52.

- [33] R.E. Coffman, G.R. Buettner, General magnetic dipolar interaction of spin-spin coupled molecular dimers. Application to an EPR spectrum of xanthine oxidase, *J. Phys. Chem.* 83 (1979) 2392–2400.
- [34] D.S. Patil, et al., EPR-detectable redox centers of the periplasmic hydrogenase from *Desulfovibrio vulgaris*, *J. Biol. Chem.* 263 (1988) 18732–18738.
- [35] J.H. Artz, et al., Reduction potentials of [FeFe]-hydrogenase accessory iron–sulfur clusters provide insights into the energetics of proton reduction catalysis, *J. Am. Chem. Soc.* 139 (2017) 9544–9550.
- [36] H.J. Grande, W.R. Dunham, B. Averill, C. van Dijk, R.H. Sands, Electron paramagnetic resonance and other properties of hydrogenases isolated from *Desulfovibrio vulgaris* (strain Hildenborough) and *Megasphaera elsdenii*, *Eur. J. Biochem.* 136 (1983) 201–207.
- [37] I.R. Vassiliev, M.L. Antonkine, J.H. Golbeck, Iron-sulfur clusters in type I reaction centers, *Biochim. Biophys. Acta* 1507 (2001) 139–160.
- [38] P. Kyritsis, O.M. Hatzfeld, T.A. Link, J.-M. Moulis, The two [4Fe-4S] clusters in *Chromatium vinosum* ferredoxin have largely different reduction potentials: structural origin and functional consequences *, *J. Biol. Chem.* 273 (1998) 15404–15411.
- [39] P.J.H. Daas, W.R. Hagen, J.T. Keltjens, G.D. Vogels, Characterization and determination of the redox properties of the 2[4Fe-4S] ferredoxin from *Methanosarcina barkeri* strain MS, *FEBS Lett.* 356 (1994) 342–344.
- [40] S.J. Maiocco, A.J. Arcinas, S.J. Booker, S.J. Elliott, Parsing redox potentials of five ferredoxins found within *Thermotoga maritima*, *Protein Sci.* 28 (2019) 257–266.
- [41] J. Hirst, Elucidating the mechanisms of coupled electron transfer and catalytic reactions by protein film voltammetry, *Biochim. Biophys. Acta (BBA) - Bioenerg.* 1757 (2006) 225–239.
- [42] R.C. Prince, M.W. Adams, Oxidation-reduction properties of the two Fe4S4 clusters in *Clostridium pasteurianum* ferredoxin, *J. Biol. Chem.* 262 (1987) 5125–5128.
- [43] H.S. Gao-Sheridan, H.R. Pershad, F.A. Armstrong, B.K. Burgess, Discovery of a novel ferredoxin from *Azotobacter vinelandii* containing two [4Fe-4S] clusters with widely differing and very negative reduction potentials, *J. Biol. Chem.* 273 (1998) 5514–5519.
- [44] J.G. Huber, J. Gaillard, J.-M. Moulis, NMR of *Chromatium vinosum* ferredoxin: evidence for structural inequivalence and impeded electron transfer between the two [4Fe-4S] clusters, *Biochemistry* 34 (1995) 194–205.
- [45] W.V. Sweeney, B.A. McIntosh, Determination of cooperative interaction between clusters in *Clostridium pasteurianum* 2 (4Fe-4S) ferredoxin, *J. Biol. Chem.* 254 (1979) 4499–4501.
- [46] D. Bontrop, I. Bertini, C. Luchinat, W. Nitschke, U. Mühlhoff, Characterization of the unbound 2[Fe4S4]-ferredoxin-like photosystem I subunit PsaC from the cyanobacterium *Synechococcus elongatus*, *Biochemistry* 36 (1997) 13629–13637.
- [47] T. Kanda, H. Ishikita, Redox potentials of iron–sulfur clusters in Type I photosynthetic reaction centers, *J. Phys. Chem. B* 127 (2023) 4998–5004.
- [48] D.A. Glauser, F. Bourquin, W. Manieri, P. Schürmann, Characterization of ferredoxin:thioredoxin reductase modified by site-directed mutagenesis, *J. Biol. Chem.* 279 (2004) 16662–16669.
- [49] B.J. Rauch, A. Gustafson, J.J. Perona, Novel proteins for homocysteine biosynthesis in anaerobic microorganisms, *Mol. Microbiol.* 94 (2014) 1330–1342.
- [50] B.J. Rauch, J. Klimek, L. David, J.J. Perona, Persulfide formation mediates cysteine and homocysteine biosynthesis in *Methanosarcina acetivorans*, *Biochemistry* 56 (2017) 1051–1061.
- [51] K.D. Allen, D.V. Miller, B.J. Rauch, J.J. Perona, R.H. White, Homocysteine is biosynthesized from aspartate semialdehyde and hydrogen sulfide in methanogenic Archaea, *Biochemistry* 54 (2015) 3129–3132.
- [52] S. Vajda, et al., New additions to the ClusPro server motivated by CAPRI, *Proteins: Struct., Funct., Bioinf.* 85 (2017) 435–444.
- [53] I.T. Desta, K.A. Porter, B. Xia, D. Kozakov, S. Vajda, Performance and its limits in rigid body protein-protein docking, *Structure* 28 (2020) 1071–1081.e1073.
- [54] S. Dai, et al., Structural snapshots along the reaction pathway of ferredoxin–thioredoxin reductase, *Nature* 448 (2007) 92–96.
- [55] P. Bohutskyi, et al., Metabolic effects of vitamin B12 on physiology, stress resistance, growth rate and biomass productivity of cyanobacterium stamierii planktonic and biofilm cultures, *Algal Res.* 42 (2019), 101580.
- [56] L. Tarrago, E. Laugier, P. Rey, Protein-repairing methionine sulfoxide reductases in photosynthetic organisms: gene organization, reduction mechanisms, and physiological roles, *Mol. Plant* 2 (2009) 202–217.
- [57] L.C. Romero, et al., Cysteine and cysteine-related signaling pathways in *Arabidopsis thaliana*, *Mol. Plant* 7 (2014) 264–276.
- [58] A.T.P. Carvalho, M. Swart, Electronic structure investigation and parametrization of biologically relevant iron–sulfur clusters, *J. Chem. Inf. Model.* 54 (2014) 613–620.
- [59] N.A. Baker, D. Sept, S. Joseph, M.J. Holst, J.A. McCammon, Electrostatics of nanosystems: application to microtubules and the ribosome, *Proc. Natl. Acad. Sci.* 98 (2001) 10037–10041.
- [60] W.W. Fish, Rapid colorimetric micromethod for the quantitation of complexed iron in biological samples, *Methods Enzymol.* 158 (1988) 357–364.
- [61] S. Stoll, A. Schweiger, EasySpin, a comprehensive software package for spectral simulation and analysis in EPR, *J. Magn. Reson.* 178 (2006) 42–55.